Novel Probabilistic Optimization Model for Lead-Acid and Vanadium Redox Flow Batteries Under Real-Time Pricing Programs

Juan M. Lujano-Rojas[a], Ghassan Zubi[b,c], Rodolfo Dufo-López[d], José L. Bernal-Agustín[d], João P. S. Catalão[a,e,f,*]

[a]INESC-ID, Instituto Superior Técnico, University of Lisbon, Av. Rovisco Pais, 1, 1049-001 Lisbon, Portugal

[b]Department for Management of Science and Technology Development, Ton Duc Thang University, Ho Chi Minh City, Vietnam.

[c]Faculty of Electrical & Electronics Engineering, Ton Duc Thang University, Ho Chi Minh City, Vietnam.

[d]Department of Electrical Engineering, Universidad de Zaragoza, Calle María de Luna 3, 50018 Zaragoza, Spain

[e]INESC TEC and Faculty of Engineering of the University of Porto, R. Dr. Roberto Frias, 4200-465 Porto, Portugal

[f]C-MAST, University of Beira Interior, R. Fonte do Lameiro, 6201-001 Covilhã, Portugal

* Corresponding author at: Faculty of Engineering of the University of Porto, R. Dr. Roberto Frias, 4200-465 Porto, Portugal. E-mail address: catalao@ubi.pt (J.P.S. Catalão).

Abstract

The integration of storage systems into smart grids is being widely analysed in order to increase the flexibility of the power system and its ability to accommodate a higher share of wind and solar power. The success of this process requires a comprehensive techno-economic study of the storage technology in contrast with electricity market behaviour. The focus of this work is on lead-acid and vanadium redox flow batteries. This paper presents a novel probabilistic optimization model for managing energy storage systems. The model is able to incorporate the forecasting error of electricity prices, offering with this a near-optimal control option. Using real data from the Spanish electricity market from the year 2016, the probability distribution of forecasting error is determined. The model determines electricity price uncertainty by means of Monte Carlo Simulation and includes it in the energy arbitrage problem, which is eventually solved by using an integer-coded genetic algorithm. In this way, the probability distribution of the revenue is determined with consideration of the complex behaviours of lead-acid and vanadium redox flow batteries as well as their associated operating devices such as power converters.

Keywords: lead-acid battery; vanadium redox flow battery; real-time pricing; genetic algorithm; smart grid.

Nomenclature

t	Index of each element of the predicted prices ($t = 1, \dots, T$).
h	Index of each element of the large-scale price database ($h = 1, \dots, H$).
p	Index of each coefficient of AR part ($p = 1, \dots, P$).

q	Index of each coefficient of MA part ($q = 1, \dots, Q$).
l	Index for each lag of autocorrelation analysis ($l = 1, \dots, L$).
m	Index for each MCS trial ($m = 1, \dots, M$).
g	Index of each generation of GA ($g = 1, \dots, G$).
k	Index of each individual of GA ($k = 1, \dots, K$).
i	Index of each individual of GA ($i = 1, \dots, I$).
b	Index of each bit of individual $\vec{a}_k$ ($b = 1, \dots, B$).
AR_p	p^{th} auto-regressive coefficient.
MA_q	q^{th} moving average coefficient.
e_h	Error of ARMA model at time h.
EP_h	Electricity price at time h (€/MWh).
EP_{min}	Minimum price of the large-scale price database (€/MWh).
EP_{max}	Maximum price of the large-scale price database (€/MWh).
TEP_h	Transformed electricity price at time h.
$TSEP_h$	Transformed and standardized electricity price at time h.
FEP_t	Forecasted electricity price at time t (€/MWh).
$FTEP_t$	Forecasted transformed electricity price at time t.
$FTSEP_t$	Forecasted transformed and standardized electricity price at time t.
Q_{stat}	Ljung-Box statistic.
r_l	Autocorrelation of the residuals at lag l.
δ	Significance level (0.05).
χ^2_δ	Chi-square distribution with $L - P - Q$ degrees of freedom and significance level δ.
F_N	CDF of a normal distribution.
F_{EP}	CDF of the large-scale price database.
$f_{FE,t}$	PDF of electricity price at time t (beta PDF).
$F_{FE,t}$	CDF of electricity price at time t (beta PDF).
α_t, β_t	Parameters of beta PDF at time t.
$f_{DA,t}$	PDF of electricity price at time t used for day-ahead prediction.
AFP	Average forecasted prices (€/MWh).
$SDFP$	Standard deviation of forecasted prices (€/MWh).
$ATEP_t$	Averaged transformed electricity price at time t.
$FEPS_{t,m}$	Forecasted electricity price scenario at time t and trial m (€/MWh).
$NFEP_t$	Normalized forecasted electricity price (€/MWh).
$NFEPS_{t,m}$	Normalized forecasted electricity price scenario at time t and trial m.
$u_{t,m}$	Correlated random variable with normal distribution.

φ	Correlation coefficient.
ξ	Non-correlated variable with normal distribution.
X	Crossover rate of GA (ARMA model).
R	Mutation rate of GA (ARMA model).
$f_{GA,s}$	Fitness function of individual s.
A	Population of GA (ARMA model).
Z	Population of GA (battery control).
$\vec{a}_k$	Individual k of GA (ARMA model).
$\vec{z}_i$	Individual i of GA (battery control).
a_b^k	Value of bit b of individual $\vec{a}_k$.
z_t^i	Control decision at time t for individual i.
NS	Number of batteries in serial.
NP	Number of batteries in parallel.
RV_i	Revenue of individual i.
$P_{SYS,t}$	Power of battery bank at time t.
$ZP_{SYS,t,i}$	Power of battery bank at time t for individual i.
$T_{A,t}$	Ambient temperature at time t (K).
T_E	Electrolyte temperature (K).
U_t	Battery voltage under general conditions (V).
U_{min}	Minimum battery voltage (V).
U_{max}	Maximum battery voltage (V).
$U_{LAB,t}^C$	Battery voltage of LAB under charging conditions (V).
$U_{LAB,t}^D$	Battery voltage of LAB under discharging conditions (V).
$U_{VRB,t}^C$	Battery voltage of VRFB under charging conditions (V).
$U_{VRB,t}^D$	Battery voltage of VRFB under discharging conditions (V).
SOC_t	SOC at time t.
SOC_{min}	Minimum SOC.
SOC_{max}	Maximum SOC.
DOD_t	DOD at time t.
I_t	Current of LAB (A).
P_t	Battery power of VRFB (kW).
C_N	Battery rated capacity (Ah for LAB and kWh for VRFB).
C_{10}	Capacity in 10h of LAB (Ah).
I_{10}	Current in 10h of LAB (A).
$I_{G,O}$	Normalized gassing current for a 100Ah battery (A).

$U_{G,O}$	Nominal voltage under gassing conditions (V).
$T_{G,O}$	Nominal temperature under gassing conditions (K).
$\eta_{INV,t}$	Efficiency of the inverter at time t.
$\eta_{V,t}^{C}$	Voltage efficiency of VRFB during charging at time t.
$\eta_{E,t}^{C}$	Power efficiency of VRFB during charging at time t.
$\eta_{VRB,t}^{C}$	Efficiency of VRFB during charging at time t.
$\eta_{V,t}^{D}$	Voltage efficiency of VRFB during discharging at time t.
$\eta_{E,t}^{D}$	Power efficiency of VRFB during discharging at time t.
$\eta_{VRB,t}^{D}$	Efficiency of VRFB during discharging at time t.
$\eta_{VRB,t}$	Efficiency of VRFB at time t.
$IP_{INV}^{1}, IP_{INV}^{2}$	Inverter parameters.
$VP_{LAB}^{1} \cdots VP_{LAB}^{12}$	Voltage parameters of LAB.
$VP_{VRB}^{1} \cdots VP_{VRB}^{7}$	Voltage parameters of VRFB.
$CP_{LAB}^{1} \cdots CP_{LAB}^{3}$	Current parameters of LAB.
$EP_{VRB}^{1} \cdots EP_{VRB}^{20}$	Efficiency parameters of VRFB.

1. Introduction

Integration of renewable energies is seen as a way to harmonize technological progress with environment conservation. However, renewable natural resources are highly variable, which directly contrasts with the operating philosophy of energy conversion systems. To solve this dilemma, the adopted option has been to increase the flexibility of the power system by incentivizing consumers to modify their consumption behaviour or by installing energy storage devices in a centralized or de-centralized manner so that the power consumption from renewable sources is enhanced.

Many efforts have been made to develop devices capable to store energy at different magnitudes. According to their technical characteristics, storing technologies can be used for different tasks of power-system operation such as integration of renewable power generation, emergency and telecommunications power support, ramping and load following, peak-shaving, and load levelling [1]. However, their economic integration into energy business and electricity markets is difficult and depends on many important factors.

Regarding the techno-economic analysis for the integration of energy storage in European Union (EU) countries, according to the results reported by Zafirakis *et al*. in [2], those electricity markets with low degree of competitiveness and highly dependent on energy imports offered the highest opportunities for the successful incorporation of energy storage. In such markets, energy imports are used to cover peak loads, which results in high peak-prices and favourable conditions for energy storage operation. The transition toward a power system strongly based on renewable energies is currently under analysis in EU countries. According to the most recent studies, pumped hydroelectric storage (PHS) can play a key role in the mitigation of power fluctuation related to wind-power generation, while other technologies such as conventional batteries and hydrogen-based storage units are not economically viable [3]. In the

United States, Bradury *et al*. [4], analysed the integration of a wide range of storage technologies in several electricity markets and concluded that economic benefit depends on charging and discharging efficiencies, the corresponding self-discharge ratios, and capacity. According to the study's results, economic benefit increases as the conversion efficiency of the corresponding storage device improves provided that it has a relevant effect on the power transaction between the storage unit and the power system. On the other hand, the storage capacity of less than half a day offers higher benefits. In addition, the volatility of electricity prices and daily behaviour are important factors because the highest revenue is obtained under peak-price conditions.

Similarly, using data from the United States, de Sisternes *et al*. [5] concluded that storage technologies are particularly required when high reduction rates of carbon dioxide (CO_2) emissions are among the main goals. This was particularly observed for conventional battery technologies with low capacity (around 2 hours), while storage units of higher magnitudes (specifically PHS- based with 10 hours of duration) were found to be suitable when massive deployment was required. In Great Britain, interesting results were reported by Dunbar *et al*. in [6], where the influence of wind power generation on electricity prices and storage-unit profitability was evaluated. According to the observed results, the incremental capacity of wind-power generation could reduce electricity prices and reduce the frequency of price spikes, reducing the benefits obtained from the operation of storage units at peak prices. On the other hand, this situation could introduce uncertainty about the profitability of storage device installation due to yearly variations in revenue. In Germany, the transition to a power system powered by clean energies has been also analysed. Weitemeyer *et al*. [7] estimated that up to 50% of electricity demand could be supplied if the power generation mix was based on wind and solar energies combined with the appropriate capacity of flexible generation units. In this way, renewable power curtailment and energy storage integration could be avoided. However, if more than 80% of electricity demand has to be supplied by clean power sources, then storage units of high efficiency and small capacity should be installed. An analysis of storage unit integration in the National Electricity Market of Australia [8] concluded that the most convenient storage capacity is around 6 hours, while the main source of economic benefit is related to the price spikes, so that storage efficiency does not play an important role.

In the specific case of conventional and flow batteries, their installation in small capacity (typically less than half a day) could be viable under very special conditions in markets with high electricity price volatility, a high share of renewable energy sources, and strict CO_2 reduction requirements.

In this context, the control of conventional and flow batteries becomes a problem that should be carefully analysed, taking into account the most important characteristics of the corresponding battery technology under analysis, as well as the electricity forecasting tools required to perform the management of stored energy in an optimal way. This problem has been widely studied in the technical literature. Powell *et al*. in [9] analysed the concept of a district energy system to take advantage of the flexibility of thermal energy storage. A storage system based on a polygeneration system is operated in order to minimize total costs on a daily basis. To solve the optimization problem, an algorithm based on the decomposition of the original optimization problem into several mixed-integer nonlinear programming (MINLP) sub-problems is introduced. The operation of a system installed in a university campus participating on the wholesale electricity market of Texas revealed a reduction of 16.5% in total costs. Tan *et al*. in [10] developed a strategy based on balancing revenue and battery lifetime through determining the Pareto optimal arbitrage policy to be applied on the control of conventional batteries. The relationship between battery lifetime and its economic performance are jointly analysed using a constrained stochastic shortest path (CSSP)

model combined with a parallel algorithm in order to determine the optimal solution. Zhang *et al*. in [11] paid special attention to the effects of charging and discharging costs on a real-time basis. Authors analysed discharging opportunity costs and marginal charging costs to include them in an operating strategy composed of two layers known as the higher layer and the lower layer. The higher layer is designed to perform a look-ahead dispatch, which is later corrected by the lower layer, improving the effectiveness of the control algorithm. Kim *et al*. in [12] studied the interaction between conventional battery operation, power system, and load consumption profile using data from an urban railway in Korea, considering time of use (TOU) tariff. Dvorkin *et al*. in [13] analysed the optimal placement and sizing of large-scale storage devices in transmission systems to reduce operating and capital costs using a mathematical model based on a bi-level strategy formulated as a mixed-integer linear programming (MILP) problem. Xu and Tong in [14] developed an optimization model based on dynamic programming (DP). Considering correlated electricity prices and load demands, an operating strategy based on two thresholds was proposed. Sakti *et al*. in [15] presented an interesting mathematical model based on the MILP approach to model conventional batteries (specifically lithium-ion batteries). The model was formulated based on basic physical phenomena such as thermodynamics, charge conduction, charge transfer at an interface, and mass transport. Geem and Yoon in [16] proposed an optimization model based on a harmony search algorithm, which was later compared with a real-coded genetic algorithm (RCGA). The effectiveness of the proposed method was verified using data from the northwest quadrant of the United States, including a TOU dynamic tariff. Wankmüller *et al*. in [17] analysed the effect of lifetime degradation of conventional batteries on revenue. Using data from Midcontinent Independent System Operator combined with two mathematical models of battery degradation, a 12–46% reduction in revenues was estimated. Moreover, incorporation of penalty costs related to this effect could improve the economic performance of the storage system. In a previous work [18], the authors studied the impact of forecasting errors and technical limitations of the power system on the operation of conventional batteries working in isolation or in aggregated form. The analysis was performed using data from the Spanish electricity market combined with detailed computational models. The optimization problem for energy arbitrage was mathematically formulated and solved using an integer-coded genetic algorithm (ICGA) able to consider the non-linear characteristics of conventional batteries. In addition, the importance of operating and dispatch analysis considering the specific characteristics of the battery under analysis, including its control devices, and the forecasting errors of the specific prediction tool, among other factors, was put in evidence.

Once the overview of storage technology integration has been presented and discussed in a wide range, the importance of an effective computational tool for continuous control and management is needed. This fact can be clearly observed by discussing the influence of the conversion efficiency. According to some studies previously described, efficiency is reported to be important or not [4,8] and influences the revenue estimations depending on how this is mathematically represented, (i.e., through a constant value or by means of a mathematical function) [15]. This panorama has motivated us to extend our previous research [18] to significantly contribute to the state of the art in several different ways, including:

- The model analysed in our previous study [18] was developed using only lead-acid batteries (LABs); in this paper, the computational model was extended to include vanadium redox flow batteries (VRFBs), as well as the electricity price forecasting error.

- Using recent information from the Spanish electricity market, from years 2015 and 2016, an optimal time series methodology was used to determine a suitable forecasting model, which is used to measure the probability distribution function (PDF) of hourly forecasting error included in the optimization problem by means of Monte Carlo simulation (MCS) approach.
- The model presented in this paper is able to estimate a near-optimal scheduling for LABs and VRFBs including the distribution of the corresponding economic benefit. Unlike previous works based on MILP, MINLP, CSSP, DP, and RCGA, an ICGA has been adopted.

The rest of the paper is organized as follows: section 2 describes the electricity price forecasting and its error, section 3 presents the mathematical models of LABs and VRFBs used, section 4 carefully presents the proposed methodology, which is later illustrated in section 5 through a case study; finally, the main conclusions are discussed in section 6.

2. Electricity price forecasting and its error

Economic management of energy corporations requires forecasts of electricity prices in order to determine and implement the appropriate operative decisions, thus ensuring the profitability and economic sustainability of the generation company [19]. In this sense, forecasting models could be categorized as multi-agent models, fundamental methods, reduced-form models, statistical approaches, computational intelligence techniques, and hybrid techniques. Multi-agent models are able to perform a price forecast by taking into account the interaction between the different generation units and specific bidding considerations commonly observed in competitive electricity markets. In fundamental methods, essential factors such as load behaviour and environmental conditions are independently predicted and later included on the price prediction model, which is formulated to consider the relationship between these factors and energy prices. Reduced-form models aim to represent the behaviour of electricity prices on a daily basis, including the energy price dynamic behaviour and correlation useful for risk management. Statistical approaches are based on the application of a mathematical relationship between past and current values to carry out the corresponding prediction; such a relationship is frequently established using econometric models. Computational intelligence techniques represent the energy price dynamic by means of the combination of heuristic approaches. Finally, hybrid techniques combine two or more of the aforementioned methodologies to improve the quality and accuracy of the price prediction [20].

In this paper, a statistical model based on an auto-regressive moving average (ARMA) model has been adopted. In addition, its ability for day-ahead forecasting has been measured in terms of the forecasting error, which has been represented by means of a beta PDF. A detailed description of the procedure required for fitting and forecasting electricity prices is explained in the next subsections.

2.1 ARMA model structure and parameterization

A general expression of the ARMA model is shown in (1), which is composed of the auto-regressive (AR) and moving average (MA) parts, presented in the first and second terms, respectively. Time series analysis requires the availability of a large-scale price database with H elements represented by the index h. As the PDF of price time series could be non-Gaussian, incorporation of a transformation process is required in order to

obtain a Gaussian distribution. Then the resulting time series is standardized, resulting in a transformed and standardized electricity price ($TSEP_h \; \forall \, h = 1, \dots H$) time series. This time series is then used to determine the order of AR (P) and MA (Q) parts, as well as the value of their coefficients ($AR_p \; \forall \, p = 1, \dots, P$ and $MA_q \; \forall \, q = 1, \dots, Q$).

$$TSEP_h = \sum_{p=1}^{P} AR_p TSEP_{h-p} + \sum_{q=1}^{Q} MA_q e_{h-q} \; \forall \, h = 1, \dots, H. \tag{1}$$

The next subsections explain the transformation and standardization, order estimation, day-ahead forecasting, and optimal fitting of ARMA models.

2.1.1 Transformation and standardization

As stated before, through transformation and standardization processes applied over the large-scale price database ($EP_h \; \forall \, h = 1, \dots, H$) results in a time series with an approximated Gaussian PDF with mean zero and standard deviation of one ($TEP_h \; \forall \, h = 1, \dots, H$). This transformation is presented in Fig. 1 and (2) [21]; to implement this transformation, the discretized cumulative density function (CDF) of electricity prices (F_{EP}) has to be estimated using the elements of the large-scale database. In addition, the CDF of a Gaussian PDF with a mean zero and standard deviation of one (F_N) is also required. On the one hand, the function F_{EP} is defined between the minimum ($EP_{min} = min\{EP_h \; \forall \, h = 1, \dots, H\}$) and the maximum ($EP_{max} = max\{EP_h \; \forall \, h = 1, \dots, H\}$) values of the large-scale database. On the other hand, a discretized version of the normalized Gaussian distribution defined in the interval $[-5,5]$ is used [22].

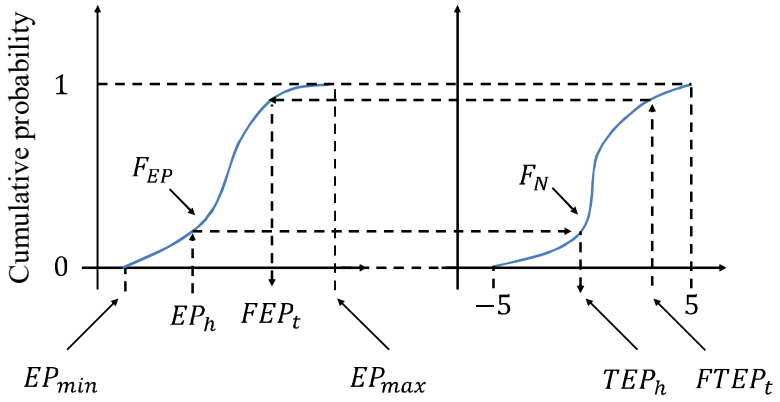

Fig. 1: Probability transformation of the electricity price database.

$$TEP_h = F_N^{-1}\big(F_{EP}(EP_h)\big) \; \forall \, h = 1, \dots, H. \tag{2}$$

Once the price database has been transformed and standardized, the diurnal stationarity is removed by subtracting the hourly average ($ATEP_t \; \forall \, t = 1, \dots, T$) as shown in (3) [23].

$$TSEP_h = TEP_h - ATEP_t \; \forall \, h = 1, \dots, H; \; t = 1, \dots, T. \tag{3}$$

Then, the order and coefficients of ARMA model can be estimated using this transformed and standardized time series.

2.1.2 Order estimation and statistical checking

Order estimation consists of determining a suitable number of elements for the AR and MA parts, represented by P and Q, respectively. This task is traditionally performed by means of the Bayesian Information Criterion (BIC) [24] or the Akaike Information Criterion (AIC) [25]. Statistical checking process is carried out to verify the quality of a determined ARMA model with P auto-regressive coefficients and Q moving average coefficients. Statistical checking is performed by using the Ljung-Box test presented in (4) [26],

$$Q_{stat} = H(H+2)\sum_{l=1}^{L}\frac{r_l^2}{H-l}; \tag{4}$$

where the statistic Q_{stat} is compared with the value of a chi-square distribution with $L-P-Q$ degrees of freedom and a significance level δ.

2.1.3 Optimal fitting of ARMA model by ICGA

In order to optimize the process of ARMA model fitting, an ICGA [27] is going to be implemented to minimize the number of coefficients $(p+q)$ and ensure the quality of the evaluated model through the application of the Ljung-Box test. Fig. 2 shows the form of the individual k of the genetic algorithm (GA) used here, where both the order of the AR part (p) and the order of the MA part (q) are represented using binary numbers. This individual could be mathematically expressed using (5) with a total number of B bits, while the variable $a_b^k \in \{0,1\}\ \forall\ b = 1,\dots,B; k = 1,\dots,K$. Finally, the population of GA (A) is represented as in (6) in matrix form.

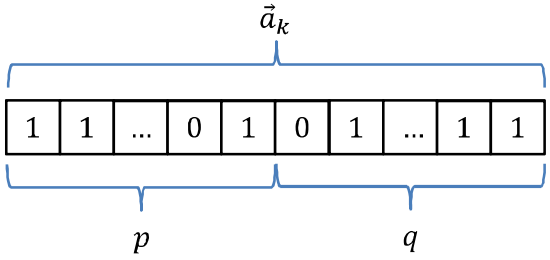

Fig. 2: Structure of individual $\vec{a}_k$ of GA.

$$\vec{a}_k = [a_1^k \quad \cdots \quad a_b^k \quad \cdots \quad a_B^k]; \tag{5}$$

$$A = \begin{bmatrix} \vec{a}_1 \\ \vdots \\ \vec{a}_k \\ \vdots \\ \vec{a}_K \end{bmatrix}. \tag{6}$$

The proposed GA for ARMA model fitting can be implemented using the following procedure:

Step 1: Estimate discretized PDF of electricity prices using the large-scale database.

Step 2: Apply the probability transformation to the large-scale electricity price database.

Step 3: Eliminate diurnal non-stationarity by subtracting the hourly average.

Step 4: Set the parameters of GA (number of generations (G), population size (K), crossover rate (X), and mutation rate (R)).

Step 5: Set the number of bits used to represent the order of AR and MA parts ($B/2$).

Step 6: Initialize the GA population (A) with binary numbers using an integer random number generator.

Step 7: Analyse the first generation by setting $g \leftarrow 1$.

Step 8.1: Evaluate the first individual by setting $k \leftarrow 1$.

Step 8.2: Using binary-to-integer numerical conversion, obtain the order of AR part (p) and MA part (q) by converting the two segments of the binary vector $\vec{a}_k$.

Step 8.3: Using the values of p and q previously obtained in Step 8.2, calculate the coefficients of the ARMA model and perform the Ljung-Box test (4). If some degree of correlation is observed, then the objective function is assigned to a value artificially high; if not, the value of objective function is assigned to $p + q$.

Step 8.4: If ($k < K$), then analyse the next individual by assigning $k \leftarrow k + 1$ and go to Step 8.2; else go to Step 8.5.

Step 8.5: To analyse the value of the objective function of the first individual, set $s \leftarrow 1$.

Step 8.6: Calculate the fitness of the s^{th} individual using (7),

$$f_{GA,s} = (K + 1 - s) / \sum_{w=1}^{K} (K + 1 - w)\,; \tag{7}$$

Step 8.7: If ($s < K$), then set $s \leftarrow s + 1$ and go to 8.6; else go to Step 8.8.

Step 8.8: Apply the reproduction, crossing, and mutation procedures according to the parameters previously defined in Step 4.

Step 8.9: If ($g < G$); then set $g \leftarrow g + 1$ and go to Step 8.1; else stop.

The individual with the highest fitness in the entire population (A) defines the order and characteristics of the ARMA model to be used on the forecasting process.

2.1.4 Day-ahead price forecasting

Using the ARMA model obtained from the implementation of the methodology described in the previous subsections, price forecasting on a daily basis can be estimated by using (8)-(10),

$$FTSEP_t = \sum_{p=1}^{P} AR_p FTSEP_t + \sum_{q=1}^{Q} MA_q e_{t-q} \;\; \forall\, t = 1, \dots, T; \tag{8}$$

$$FTEP_t = FTSEP_t + ATEP_t \;\forall\, t = 1, \dots, T; \tag{9}$$

$$FEP_t = F_{EP}^{-1}\big(F_N(FTEP_t)\big) \;\forall\, t = 1, \dots, T. \tag{10}$$

In (8), transformed and standardized daily forecasting is calculated, resulting in a vector with Gaussian PDF. Then in (9), the diurnal stationarity is added, while the forecasting profile is finally obtained from the application of the probability transformation previously explained in subsection 2.1.1 (Fig. 1) and mathematically expressed in (10). Analytical representation of forecasting error that accompanies the corresponding prediction is carefully described in the next subsection.

2.2 PDF of forecasting error and its measurement

In general, many PDFs have been suggested in the literature to represent the forecasting error of a determined mathematical model, as well as the confidence interval related to such distribution; in this way, the values to be forecasted and their uncertainty can be quantitatively estimated. Recently, several theoretical methods have been created to predict confidence intervals. For instance, the factor quantile regression averaging approach [28] is appropriate for dealing with the selection of a set of models to be combined in the forecasting process, as well as the accurate determination of prediction intervals. On the other hand, spatial interpolation techniques have been also suggested in the literature [29] to estimate several possible price conditions from the combination of probabilistic information related to uncertain variables and a wholesale electricity market equilibrium model.

In this paper, the forecasting model previously described in subsection 2.1.4 has been evaluated using a large amount of electricity price data in order to measure the characteristics of PDF forecasting error for each hour; specifically, a standard beta PDF has been used to represent such error. Fig. 3 describes the form of PDF used (shaded area), the PDFs $f_{FE,t}\ \forall\ t = 1, \dots, T$ are obtained from the evaluation of the ARMA model over the large-scale price database and they are modelled as beta PDFs. These PDFs are then truncated between the minimum ($EP_{min}\ \forall\ t = 1, \dots, T$) and maximum ($EP_{max}\ \forall\ t = 1, \dots, T$) prices observed on the large-scale database in order to estimate a tight confidence interval. The truncated distributions have been identified using the variable $f_{DA,t}\ \forall\ t = 1, \dots, T$, which is mathematically described in (11) and represented by the shaded area in Fig. 3,

$$f_{DA,t}(FEP_t) = \begin{cases} 0, FEP_t < EP_{min} \\ F_{FE,t}(EP_{min}), FEP_t = EP_{min} \\ f_{FE,t}(FEP_t), EP_{max} > FEP_t > EP_{min} \\ 1 - F_{FE,t}(EP_{max}), FEP_t = EP_{max} \\ 0, FEP_t > EP_{max} \end{cases}. \tag{11}$$

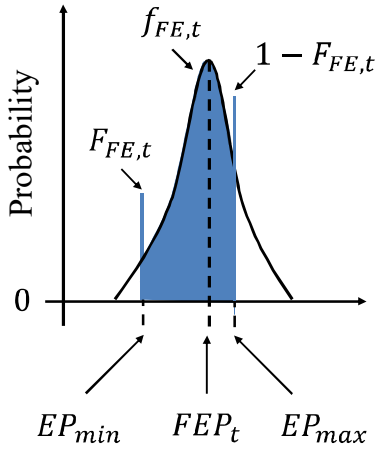

Fig. 3: PDF of forecasting error.

2.3 MCS approach for representing prediction error

Uncertainty could be modelled using an analytical version of the PDF that represents the error; however, in our problem where an entire day is analysed (T = 24 h), the analytical representation of such multivariable distribution is overwhelming due to the high number of combinations and possible cases involved. In this sense, several scenarios are randomly generated by means of copula theory according to the algorithm described below [30]:

Step 1: Perform the electricity price prediction for the day of interest.

Step 2: Using the large-scale price database, determine the parameters of forecasting error PDF at each hour $t = 1, \dots, T$.

Step 3: Calculate the one-lag correlation coefficient using the large-scale price database.

Step 4: Define the number of MCSs (M) to be generated.

Step 5: Calculate the normalized forecasted electricity prices using (12),

$$NFEP_t = \frac{FEP_t - AFP}{SDFP} \; \forall \, t = 1, \dots, T; \tag{12}$$

where AFP and $SDFP$ are the mean and standard deviation of forecasted electricity prices ($FEP_t \; \forall \, t = 1, \dots, T$), respectively.

Step 6: Generate M correlated random vectors using (13),

$$u_{t,m} = u_{t-1,m}\varphi + \xi \; \forall \, t = 1, \dots, T; m = 1, \dots, M; \tag{13}$$

Step 7: Calculate M correlated random vectors following the forecasted electricity price profile using the results obtained in Step 6 combined with (14),

$$NFEPS_{t,m} = u_{t,m} + NFEP_t \; \forall \, t = 1, \dots, T; m = 1, \dots, M; \tag{14}$$

Step 8: Using the forecasting error PDF estimated in Step 2, apply a probability transformation similar to that shown in Fig. 1 over each of the M vectors previously obtained in Step 7 in order to finally calculate the required MCSs ($FEPS_{t,m} \; \forall \, t = 1, \dots, T; m = 1, \dots, M$). Such probability transformation is described in (15),

$$FEPS_{t,m} = f_{DA,t}^{-1}\left(F_N\left(NFEPS_{t,m}\right)\right) \; \forall \, t = 1, \dots, T. \tag{15}$$

3. Battery energy storage system model

In this paper we paid special attention to LABs and VRFBs due to their technical characteristics, which make them appropriate to be installed in a distributed way [31]. The control of storage system developed in this work considers the charging and discharging power as the control variables. The state variables of storage system are the battery bank voltage and its state of charge. Technical constraints related to the operating limits of state of charge, battery voltage as well as battery power, which are values frequently suggested by the manufacturers according to the corresponding technology, are also incorporated into the optimization model as mathematical constraints. Next subsections carefully describe the model computationally implemented to represent these storage technologies in a dynamic electricity pricing paradigm.

3.1 Lead-acid battery model

LABs have been extensively used and studied for energy support in remote areas. A completed mathematical model derived from the modification of Shepherd equations was developed and presented in [32]. This is a general representation of a typical 2V cell, whose capacity (C_N) is frequently reported as the discharging capacity in 10 h (C_{10}) in Ah units. This formulation was developed in order to consider the effects of open-circuit voltage when the battery is totally charged, as well as its variations with state of charge (SOC); in addition to these aspects, the ohmic losses are also taken into account. LAB behaviour is analysed for charging ($I_t > 0 \; \forall \; t = 1, \dots, T$) and discharging ($I_t < 0 \; \forall \; t = 1, \dots, T$) processes separately, as shown in (16) for battery voltage estimation.

$$U_t = \begin{cases} U_{LAB,t}^{C};\; I_t > 0 \\ U_{LAB,t}^{D};\; I_t \leq 0 \end{cases} \forall \; t = 1, \dots, T. \tag{16}$$

During charging conditions, LAB voltage is calculated by using (17); while under discharging, this is calculated as shown in (18). Regarding SOC and depth of discharge (DOD) estimation, this can be carried out using (19)-(21), where the impact of the gassing current is considered.

$$U_{LAB,t}^{C} = VP_{LAB}^{1} - VP_{LAB}^{2}(DOD_t) + VP_{LAB}^{3}\left(\frac{I_t}{C_N}\right) + VP_{LAB}^{4} VP_{LAB}^{5}\left(\frac{I_t}{C_N}\right)\left(\frac{SOC_t}{VP_{LAB}^{6} - SOC_t}\right); \; I_t > 0 \; \forall \; t = 1, \dots, T; \tag{17}$$

$$U_{LAB,t}^{D} = VP_{LAB}^{7} - VP_{LAB}^{8}(DOD_t) + VP_{LAB}^{9}\left(\frac{I_t}{C_N}\right) + VP_{LAB}^{10} VP_{LAB}^{11}\left(\frac{I_t}{C_N}\right)\left(\frac{DOD_t}{VP_{LAB}^{12} - DOD_t}\right); \; I_t \leq 0 \; \forall \; t = 1, \dots, T. \tag{18}$$

$$SOC_t = SOC_{t-1} + \int_{t-1}^{t} \left(\frac{I_\tau - I_{G,\tau}}{C_N}\right) d\tau \; \forall \; t = 1, \dots, T; \tag{19}$$

$$DOD_t = 1 - SOC_t \; \forall \; t = 1, \dots, T; \tag{20}$$

$$I_{G,t} = \left(\frac{C_N}{CP_{LAB}^{1}}\right)(I_{G,O}) exp\left(CP_{LAB}^{2}\left[U_t - U_{G,O}\right] + CP_{LAB}^{3}\left[T_{A,t} - T_{G,O}\right]\right) \; \forall \; t = 1, \dots, T; \tag{21}$$

In Tables 1 and 2 [32], the parameters of a typical flat-plate battery (OGi) with a flooded electrolyte are presented; this technology is frequently recommended by several manufacturers for photovoltaic systems.

Table 1: Parameters of LAB model (Battery voltage).

Parameter	Value	Parameter	Value
VP_{LAB}^{1}	2.1 V	VP_{LAB}^{7}	2.1 V
VP_{LAB}^{2}	0.076 V	VP_{LAB}^{8}	0.076 V
VP_{LAB}^{3}	0.42 ΩAh	VP_{LAB}^{9}	0.699 ΩAh
VP_{LAB}^{4}	0.42 ΩAh	VP_{LAB}^{10}	0.699 ΩAh
VP_{LAB}^{5}	0.888	VP_{LAB}^{11}	0.0464
VP_{LAB}^{6}	1.001	VP_{LAB}^{12}	1.75

Table 2: Parameters of LAB model (Battery current and SOC).

Parameter	Value	Parameter	Value
CP_{LAB}^{1}	100 Ah	$I_{G,O}$	0.020 A
CP_{LAB}^{2}	11 1/V	$U_{G,O}$	2.23 V
CP_{LAB}^{3}	0.06 1/K	$T_{G,O}$	298 K

3.2 Vanadium redox flow battery model

VRFB is a promising technology to be integrated in a distributed way for energy storage at the residential level. As in the case of the LAB modelling previously described, a typical battery of 5 kW, 20 kWh, and 50 V was adopted. This model has been experimentally measured and characterized in [33]-[35]; however, additional information about this technology can be found [36]. The behaviour of this battery is expressed in terms of charging ($P_t > 0 \; \forall \; t = 1, \dots, T$) or discharging ($P_t < 0 \; \forall \; t = 1, \dots, T$) power as expressed in (22) and (23), where battery voltage and its efficiency have been considered.

$$U_t = \begin{cases} U_{VRB,t}^{C};\ P_t > 0 \\ U_{VRB,t}^{D};\ P_t \leq 0 \end{cases} \forall\ t = 1, \dots, T; \tag{22}$$

$$\eta_{VRB,t} = \begin{cases} \eta_{VRB,t}^{C};\ P_t > 0 \\ \eta_{VRB,t}^{D};\ P_t < 0 \end{cases} \forall\ t = 1, \dots, T. \tag{23}$$

During charging and discharging processes; battery voltage, as well as voltage and power efficiencies as a function of SOC and battery power are shown in (24)-(31) for the typical 5 kW/20 kWh battery [34]. Equations (24)-(27) model the charging process, while equations (28)-(31) represent the battery discharging process. Once conversion efficiency has been determined, SOC can be estimated using (32).

$$U_{VRB,t}^{C} = (VP_{VRB}^{1} SOC_t + VP_{VRB}^{2}) P_t + VP_{VRB}^{3} SOC_t + VP_{VRB}^{4} \; \forall\ t = 1, \dots, T; \tag{24}$$

$$\eta_{V,t}^{C} = \frac{EP_{VRB}^{1} T_E (SOC_t - EP_{VRB}^{2}) + EP_{VRB}^{3}}{(EP_{VRB}^{4} SOC_t + EP_{VRB}^{5}) P_t + EP_{VRB}^{6} SOC_t + EP_{VRB}^{7}} \; \forall\ t = 1, \dots, T; \tag{25}$$

$$\eta_{E,t}^{C} = \frac{(EP_{VRB}^{8} SOC_t + EP_{VRB}^{9}) P_t + EP_{VRB}^{10} SOC_t - EP_{VRB}^{11}}{P_t} \; \forall\ t = 1, \dots, T; \tag{26}$$

$$\eta_{VRB,t}^{C} = \eta_{V,t}^{C} \eta_{E,t}^{C} \; \forall\ t = 1, \dots, T; \tag{27}$$

$$U^{D}_{VRB,t} = VP^{5}_{VRB}|P_t| + VP^{6}_{VRB}SOC_t + VP^{7}_{VRB} \; \forall \; t = 1, \dots, T; \tag{28}$$

$$\eta^{D}_{V,t} = \frac{EP^{12}_{VRB}|P_t| + EP^{13}_{VRB}SOC_t + EP^{14}_{VRB}}{EP^{15}_{VRB}T_E(SOC_t - EP^{16}_{VRB}) + EP^{17}_{VRB}} \; \forall \; t = 1, \dots, T; \tag{29}$$

$$\eta^{D}_{E,t} = \frac{|P_t|}{EP^{18}_{VRB}|P_t| + EP^{19}_{VRB}SOC_t(SOC_t - 1) + EP^{20}_{VRB}} \; \forall \; t = 1, \dots, T; \tag{30}$$

$$\eta^{D}_{VRB,t} = \eta^{D}_{V,t}\eta^{D}_{E,t} \; \forall \; t = 1, \dots, T; \tag{31}$$

$$SOC_t = SOC_{t-1} + \int_{t-1}^{t} \left(\frac{P_\tau \eta_{VRB,t}}{C_N}\right) d\tau \; \forall \; t = 1, \dots, T. \tag{32}$$

Table 3 and 4 shows the parameters required for the 5 kW/20 kWh battery representation [34], including battery voltage, as well as voltage and power efficiencies.

Table 3: Parameters of VRFB model (battery voltage and power inverter).

Parameter	Value	Parameter	Value
VP^{1}_{VRB}	1.895 V/kW	VP^{6}_{VRB}	6.3606 V
VP^{2}_{VRB}	1.552 V/kW	VP^{7}_{VRB}	47.335 V
VP^{3}_{VRB}	6.82 V	T_E	298.15 K
VP^{4}_{VRB}	46.79 V	IP^{1}_{INV}	0.015784
VP^{5}_{VRB}	-2.72 V/kW	IP^{2}_{INV}	0.078815

Table 4: Parameters of VRFB model (battery efficiency).

Parameter	Value	Parameter	Value
EP^{1}_{VRB}	0.038 V/K	EP^{11}_{VRB}	0.59 kW
EP^{2}_{VRB}	1.1755	EP^{12}_{VRB}	-2.72 V/kW
EP^{3}_{VRB}	61.2674 V	EP^{13}_{VRB}	6.3606 V
EP^{4}_{VRB}	1.895 V/kW	EP^{14}_{VRB}	47.335 V
EP^{5}_{VRB}	1.552 V/kW	EP^{15}_{VRB}	0.038 V/K
EP^{6}_{VRB}	6.82 V	EP^{16}_{VRB}	1.1755
EP^{7}_{VRB}	46.79 V	EP^{17}_{VRB}	61.2674 V
EP^{8}_{VRB}	-0.128	EP^{18}_{VRB}	1.0334
EP^{9}_{VRB}	1.05	EP^{19}_{VRB}	1.727 kW
EP^{10}_{VRB}	0.19 kW	EP^{20}_{VRB}	0.596 kW

3.3 Charge controller model

Conversion between alternating current (AC) and direct current (DC) is carried out using a power converter; the efficiency of this device varies according to the amount of power under conversion. Typically, efficiency decreases as the power to be converted is reduced according to (33). Using this expression, the power to be taken from or sent to the smart grid (SG) ($P_{SYS,t}\ \forall\ t = 1, \dots, T$) can be calculated through (34),

$$\eta_{INV,t} = \frac{|P_t|}{IP_{INV}^1(P_{INV}^N) + (1 + IP_{INV}^2)|P_t|}\ \forall\ t = 1, \dots, T; \tag{33}$$

$$P_{SYS,t} = \pm\frac{|P_t| - IP_{INV}^1(P_{INV}^N)}{(1 + IP_{INV}^2)}\ \forall\ t = 1, \dots, T. \tag{34}$$

Parameters required to model power converter efficiency are reported in Table 3, obtained from the laboratory results previously published by Rampinelli *et al.* in [37]. The storage system models presented in subsections 3.1 and 3.2 can be scaled using several batteries connected serially (NS) and in parallel (NP) in order to complete a determined storing capacity.

3.4 Energy storage operating strategy

Fig. 4 shows a simplified representation of the battery storage incorporated to SG. Under real-time pricing, it is assumed that energy prices are available to residential consumers at each hour; distributed generators and storage systems interact with SG through the smart meter; then, the battery bank is continuously supervised by a control system that measures its voltage, power, and SOC in order to maintain these variables within acceptable values.

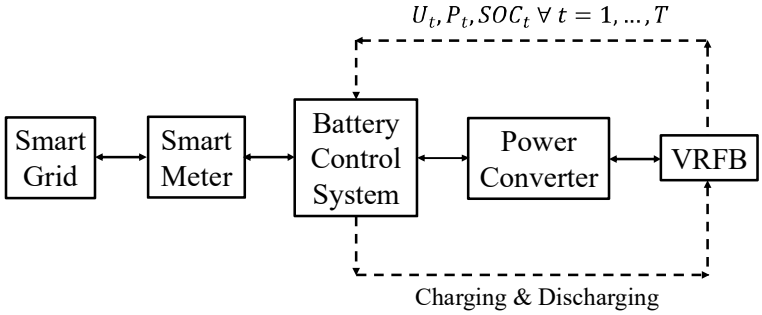

Fig. 4: VRFB integrated to SG.

A key device for battery operation is the charge controller (included in Fig. 4 in the battery control system block); this element controls the battery current and power in order to maintain the battery voltage and SOC within determined values frequently suggested by the manufacturers. In fact, the charge controller is responsible for the implementation of bulk, absorption, and float stages required during charging process. The limit values used in this work for the operation of LABs and VRFBs are presented in Table 5.

Table 5: Limit values for battery operation [32]-[35].

Control variable	LAB	VRFB
SOC_{min}	0.3	0.15
SOC_{max}	1	0.9
U_{min}	1.9 V	42V
U_{max}	2.23 V	56.5 V

Nguyen *et al.* in [34] experimentally measured and mathematically formulated the power to be applied during charging process as a function of SOC and voltage settings. Alternatively, another option consists of using the mathematical model previously formulated in subsections 3.1–3.3 to determine the appropriate power to be charged or discharged to or from the battery. LAB control has been extensively analysed in our previous research [18]; however, with the increasing interest in VRFBs, we pay special attention to its modelling and control.

During VRFB charging, two main procedures are needed. First, the maximum charging power to be applied in order to take the actual value of SOC (SOC_{t-1}) to its maximum value (SOC_{max}) is estimated using (25)-(27), and (32). In the second step, the maximum charging power previously calculated is used as a new limit constraint in the estimation of the power to be injected so that the battery voltage is less than or equal to its maximum value (U_{max}); in this procedure, VRFB is fully incorporated using (24)-(27) and (32). Note that, in the first step, only the voltage and power efficiencies are included regardless of battery voltage. This gives us a first constraint to the battery power or, in other words, an approximation of the maximum power to be applied. This result is then used to determine the proper power value by incorporating the battery voltage. A similar strategy is followed during the VRFB discharging process, the maximum power to be discharged is first estimated in order to take the SOC from the actual condition (SOC_{t-1}) to its minimum value (SOC_{min}). This is carried out using (29)-(31) and (32). In the second step, the maximum discharging power previously calculated is used as a new limit constraint in the estimation of the power to be taken so that the battery voltage is higher than or equal to its minimum value (U_{min}). In this procedure, VRFB is fully incorporated using (28)-(31) and (32). Another important point to take into consideration is that charging and discharging power are both calculated from an interval so that the non-linear algebraic equations involved in the simulation can be solved by means of a bisection method.

4. Proposed methodology

4.1 Deterministic management of LABs and VRFBs

Under deterministic assumptions, when only a specific forecasting profile is considered, battery systems can be managed using an ICGA [18] in which operating decisions are represented by means of three integer numbers, -1 to represent the discharging process, 0 to represent battery disconnection, and 1 to represent the charging process. The form of a determined individual i ($i = 1, \dots, I$) is shown in (35), where $z_t^i \in \{-1,0,1\}$. The corresponding population (Z) to which the individual z_t^i belongs to is shown in (36).

$$\vec{z}_i = \begin{bmatrix} z_1^i & \cdots & z_t^i & \cdots & z_T^i \end{bmatrix} \forall\, i = 1, \dots I; \tag{35}$$

$$Z = \begin{bmatrix} \vec{z}_1 \\ \vdots \\ \vec{z}_i \\ \vdots \\ \vec{z}_I \end{bmatrix}. \tag{36}$$

Revenue ($RV_i \;\forall\, i = 1, \dots, I$) obtained from the implementation of the control policy represented by the individual i ($\vec{z}_i \;\forall\, i = 1, \dots, I$) is computed according to (37), where the forecasted electricity prices ($FEP_t \;\forall\, t = 1, \dots, T$), as well as the charging and discharging ($ZP_{SYS,t,i} \;\forall\, t = 1, \dots, T; i = 1, \dots, I$) have been considered. It should be highlighted that $ZP_{SYS,t,i}$ is calculated in the same way as the variable $P_{SYS,t}$ through (34). These variables only differ on the index i; however, both of them have the same value.

$$RV_i = \sum_{t=1}^{T} (FEP_t)\left(ZP_{SYS,t,i}\right) \;\forall\, i = 1, \dots, I. \tag{37}$$

The optimization problem consists of finding the control policy (charging, discharging, or disconnection of the storage system) that minimizes the objective shown in (37); it should be highlighted that according to the convention of positive battery power for charging and negative battery power for discharging, the battery system obtains the highest economic benefit when the objective (RV_i) becomes negative. More details can be found in our previous study [18].

4.2 Probabilistic Management of LABs and VRFBs

Under uncertain conditions, the optimization problem to be solved consists on finding the scheduling of the battery bank in order to maximize the economic benefit, taking into account the influence of all the scenarios considered (scenarios used to represent the uncertainty associated to the electricity price forecasting). This task is performed by analyzing each scenario individually (as explained in sub-section 4.1), obtaining the control action (charging, discharging, or battery bank disconnection) with the highest probability of maximize the economic benefit. In other words, considering a determined type of battery bank (LAB or VRFB), a determined forecasting tool (ARMA model) and its associated forecasting error, the problem consists on determining the control action ($BS_t \;\forall\, t = 1, \dots, T$), so that the resulting probability distribution of economic revenue contains on its confidence interval the maximum benefit under actual conditions. The GA originally proposed in our previous work [18] has to be modified in order to consider the uncertainty introduced by the forecasting error of electricity prices. Such modification is achieved by implementing the algorithm explained as follows:

Step 1: Set a determined number of MCSs (M).

Step 2: Perform the electricity price forecasting and generate M scenarios according to section 2.

Step 3: Create three vectors initialized to zero in order to represent the probability of charging ($f_{BS,t}(BS_t = 1)$), discharging ($f_{BS,t}(BS_t = -1)$), and disconnection ($f_{BS,t}(BS_t = 0)$) of the storage system.

Step 4: Analyse the first scenario by setting $d \leftarrow 1$.

Step 5: Determine the scheduling of the storage system using the GA described in subsection 4.1 [18].

Step 6: Analyse the decisions obtained from Step 5 at each time step $t = 1, \dots, T$. If the decision obtained at time t corresponds to the charging process, then increment the probability of the vector created in Step 3 in $1/M$. If the decision corresponds to the discharging process, then increment the value of the corresponding vector in $1/M$; a similar procedure should be followed with regard to the battery disconnection decision.

Step 7: If $(m < M)$; then set $m \leftarrow m + 1$ and go to Step 5, else go to Step 8.

Step 8: From Step 7, a probabilistic matrix similar to that shown in Fig. 5 is going to be obtained. Using this matrix, the definitive control decision is derived from that condition with the highest probability (statistical mode). For example, in Fig. 5, at time t, the decision that corresponds to the charging process should be taken because it has 80% probability of being required for operation.

t	$f_{BS,t}(BS_t = 1)$	$f_{BS,t}(BS_t = -1)$	$f_{BS,t}(BS_t = 0)$	BS_t
1	⋮	⋮	⋮	⋮
⋮				
t	0.8	0.1	0.1	1
⋮	⋮	⋮	⋮	⋮
T				

Fig. 5: Matrix of probabilistic optimization.

The probabilistic methodology proposed in this research work for the control of LABs and VRFBs is illustrated using a case study, which is carefully explained in the next section.

5. Case study

In this section, we illustrate the proposed methodology through the analysis of a case study of a battery bank operating in the Spanish electricity market [38], specifically, on January 5th, 2017. The large-scale price database ($EP_h \; \forall \; h = 1, \dots H$) consists of the time series from December 1st, 2015 to January 4th, 2017. Two different battery technologies, LAB and VRFB, have been analysed and modelled according to section 3. For these battery banks (one based on LABs and another one based on VRFBs), 10 batteries connected serially and 100 batteries connected in parallel (NS=10 and NP=100) have been considered. The initial SOC (before $t = 1$) was assumed to be equal to the minimum suggested value for each technology.

In the case of battery bank based on VRFBs, this is supposed to be built from the connection of several 5 kW/20 kWh batteries. It is important to highlight that 20 kWh is the amount of effective energy to be stored on the system, so the system's maximum capacity (C_N) is estimated as 26.6667kWh ($C_N[SOC_{max} - SOC_{min}]$ = 20 kWh). The total capacity of the battery bank is estimated at 2 MWh, while its maximum power is estimated at 500 kW. Regarding the battery bank based on LABs, this is supposed to be built from the connection of several batteries with a rated capacity ($C_N = C_{10}$) of 1430 Ah in order to have a total capacity of 2 MWh (C_N=2MWh/[2V$(NS)(NP)$(1-

SOC_{min})]≈1430Ah). The maximum battery current was assumed to be equal to the battery current in 10 h (I_{10}), whereas the rated voltage of the bank is 20 V.

Operating constraints shown in Table 5 related to battery voltage and SOC limits were also considered. In the next subsections, the ARMA model estimation, energy price prediction, and battery bank control for our case study are going to be analysed thoroughly. A general value for significance level of 5% was assumed (δ = 5%). Regarding the ambient temperature profile, it was assumed to be constant and equal to 298 K ($T_{A,t}$=298 K $\forall\, t = 1, \ldots, 24$).

Forecasting, simulation, and optimization models were implemented in a personal computer with i7-3630QM CPU at 2.4 GHz with 8 GB of memory and a 64-bit operating system. In addition, the computational language used was MATLAB©.

5.1 ARMA model fitting for Spanish market during 2015 and 2016

As an example of the process required for the fitting and estimation of the ARMA model using a large-scale database, the results obtained from the analysis of December 2015 are shown in Fig. 6-9. Fig. 6 and 7 show the partial and simple autocorrelation functions, and Fig. 8 illustrates discretized PDFs of the transformed and standardized time series ($TSEP_h$ $\forall\, h = 1, \ldots, H$), which was built using 250 intervals and shows a PDF distribution that is approximately Gaussian. The fitting procedure described in subsection 2.1.3 was implemented by considering 15 generations (G = 15), 50 individuals (K = 50), a crossover rate of 95% (X=95%), and a mutation rate of 5% (R = 5%). Each individual was represented using 12 bits (B = 12), so that a maximum order of 63 coefficients for AR and MA parts can be chosen. Fig. 9 presents the evolution of the GA, which converges to an ARMA model with 10 coefficients. Table 6 shows the results obtained from December 2015 to December 2016, including the number of parameters and the statistical checking.

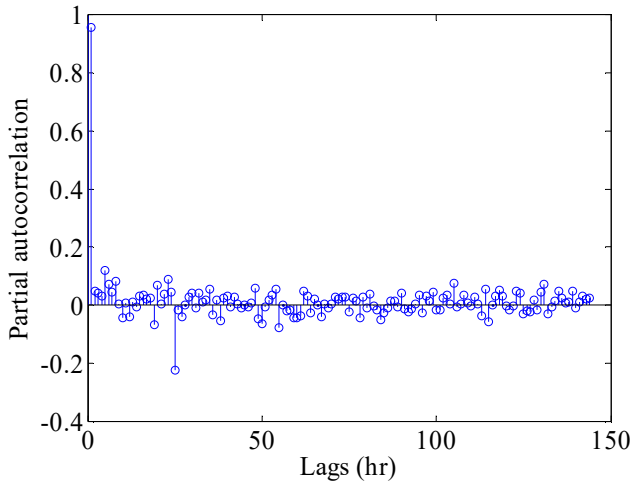

Fig. 6: Partial autocorrelation function (December 2015).

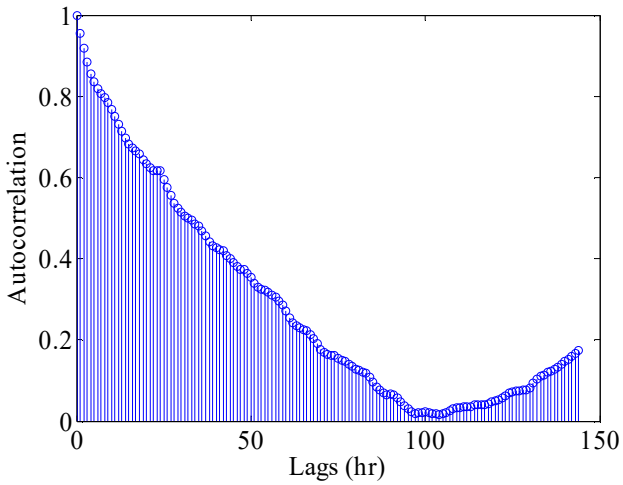

Fig. 7: Simple autocorrelation function (December 2015).

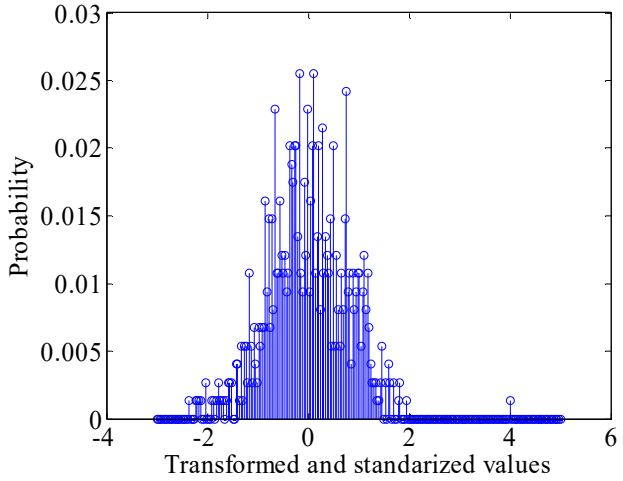

Fig. 8: PDF of transformed and standardized time series (December 2015).

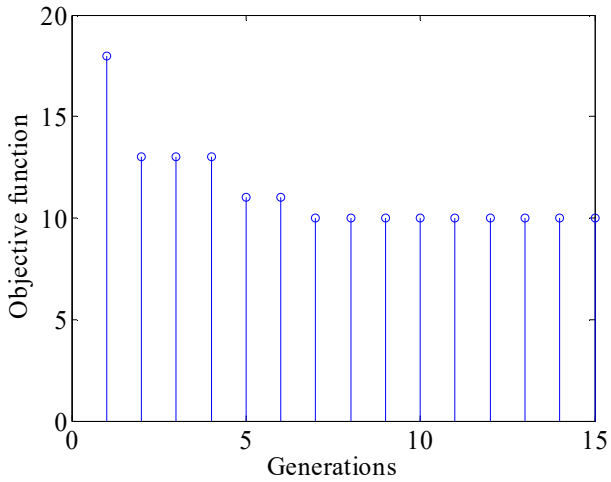

Fig. 9: Convergence of GA (December 2015).

Table 6: ARMA model fitting for 2015 and 2016.

Year	Month	P	Q	$L-P-Q$	Q_{stat}	χ^2_δ
2015	Dec	2	8	134	156.9008	162.0156
2016	Jan	1	2	141	147.0294	169.7113
	Feb	4	4	136	156.8868	164.2162
	Mar	6	2	136	161.0417	164.2162
	Apr	10	21	113	136.5337	138.8114
	May	3	0	141	157.0895	169.7113
	June	7	24	113	131.9534	138.8114
	July	8	4	132	148.8228	159.8135
	Aug	6	0	138	163.1772	166.4153
	Sept	12	6	126	147.2023	153.1979
	Oct	4	20	120	140.615	146.5674
	Nov	5	4	135	163.0477	163.1161
	Dec	5	8	131	153.3704	158.7119

Using the characteristics of the ARMA models shown in Table 6, forecasting error was determined by evaluating the model explained in subsection 2.1.4 over the year 2016. For example, the forecasting-error time series of January 2016 was measured by evaluating the ARMA model of the previous month (December 2015). This procedure was sequentially applied for every month of the year 2016, resulting in a representative time series of forecasting error.

Finally, a discretized PDF of forecasting error for each time step $t = 1, \dots, T$ was built using 250 intervals and the corresponding parameters of beta PDF (α_t and $\beta_t \; \forall \; t = 1, \dots, T$) were found, these parameters are presented in Table 7. It is important to pay attention to the fact that the forecasting-error time series was normalized to have values within the interval [0, 1] by applying a linear relationship with the minimum and maximum values shown in the Table 7 caption.

Table 7: PDF of forecasting error

(Minimum -22.529071 and maximum 38.6241888).

t	α_t	β_t
1	30.43776	51.19635
2	23.7881	39.97743
3	20.60996	35.03246
4	18.70024	31.72744
5	15.63682	26.70307
6	10.63028	18.33883
7	7.020232	11.92807
8	5.076296	8.287134
9	4.459585	7.256877
10	3.611737	5.577152
11	5.895707	9.531455
12	6.796847	11.09506
13	6.985656	11.4902
14	6.600518	10.927
15	6.133457	10.20937
16	5.358248	8.918988
17	5.045798	8.35324
18	5.492391	8.96503
19	5.506971	8.784628
20	6.135035	9.799125
21	4.323731	7.095468
22	6.298924	10.42099
23	7.851146	13.2495
24	7.260967	12.28328

5.2 Price forecasting for January 5th, 2017

Using the ARMA model of December 2016 combined with data from December 2016 and January 2017, energy prices for January 5th, 2017 were predicted. In addition, 300 price scenarios were generated using the MCS approach as explained in subsection 2.3 and considering the one-lag autocorrelation coefficient (φ) to be 0.9234. The results are shown in Fig. 10, the grey lines represent all the scenarios generated while the black line represents the actual values of the electricity market. It is possible to observe how the minimum (EP_{min}=35.2 €/MWh≈35 €/MWh) and maximum (EP_{max}=75.5 €/MWh≈76 €/MWh) energy prices lead to a tight price forecasting.

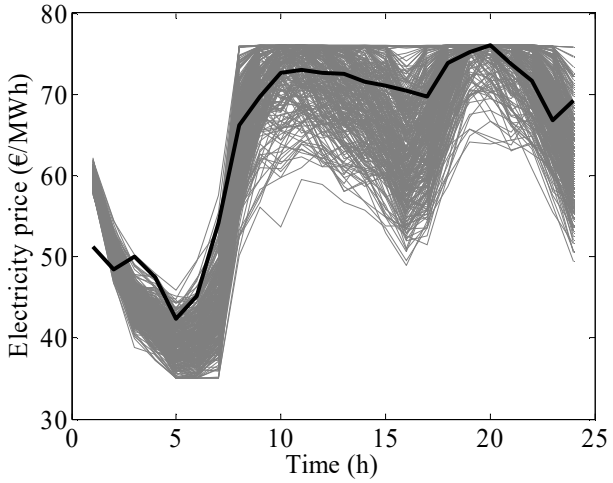

Fig. 10: Scenarios and actual energy prices (1/5/2017).

The next subsections describe the scheduling process of LAB and VRFB banks, including the impact of forecasting error on storage-system operation.

5.3 Control of LAB for January 5th, 2017

Using similar parameters to those employed for the ARMA model fitting reported in subsection 5.1 and the scenarios generated in subsection 5.2, control of LAB was performed, obtaining the matrix shown in Table 8. In this matrix, it is possible to observe that, during some hours (t = 4,…,7), the battery bank has to be charged regardless of the price uncertainty. This time frame corresponds to those hours with energy prices close to the minimum historical value. On the other hand, the probability of battery discharging reached its highest value when energy prices reached a value close the maximum historical level; specifically, during the time frame between t = 19 and t = 20.

The dynamic behaviour of the LAB bank is shown in Figs. 11–13, this was obtained by taking into consideration the operating scheduling reported in the last column of Table 8 ($BS_t \; \forall \; t = 1, \ldots, 24$). From these results, it is possible to note that the battery bank should be charged during the valley hours in order to later be discharged during high-price hours. In this sense, the formulation and solution of the control problem in a probabilistic way allows us to determine charging and discharging periods accurately.

Fig. 14 shows the probability mass function of economic benefit obtained from the operation of the LAB bank for the day in question, which is highly influenced by the PDF of forecasting error, modelled as a beta distribution.

Table 8: Matrix of probabilistic optimization (LAB).

t	$f_{BS,t}(BS_t = 1)$	$f_{BS,t}(BS_t = -1)$	$f_{BS,t}(BS_t = 0)$	BS_t
1	0	0.5133	0.4866	-1
2	0.9533	0.0200	0.0266	1
3	0.9966	0	0.0033	1
4	1	0	0	1
5	1	0	0	1
6	1	0	0	1
7	1	0	0	1
8	0.6366	0.0833	0.2800	1
9	0.0866	0.6566	0.2566	-1
10	0.0433	0.8200	0.1366	-1
11	0.0266	0.8366	0.1366	-1
12	0.0266	0.7466	0.2266	-1
13	0.0600	0.5233	0.4166	-1
14	0.1400	0.3733	0.4866	0
15	0.3700	0.2200	0.4100	0
16	0.7766	0.0766	0.1466	1
17	0.5433	0.1433	0.3133	1
18	0.0233	0.5266	0.4500	-1
19	0	0.9133	0.0866	-1
20	0	0.9333	0.0666	-1
21	0	0.8366	0.1633	-1
22	0	0.8500	0.1500	-1
23	0	0.7400	0.2600	-1
24	0	0.6066	0.3933	-1

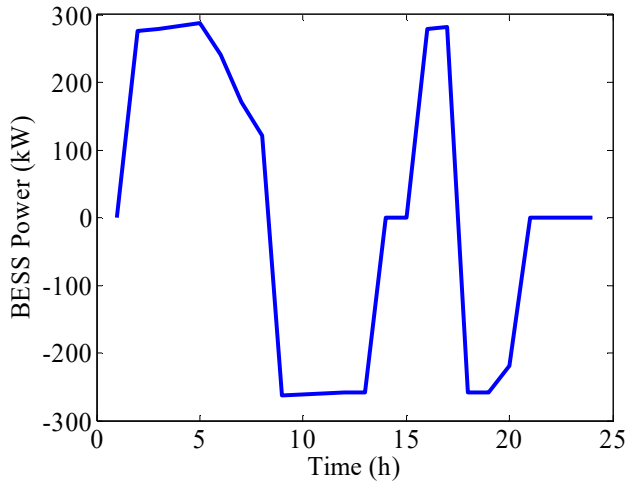

Fig. 11: LAB power (1/5/2017).

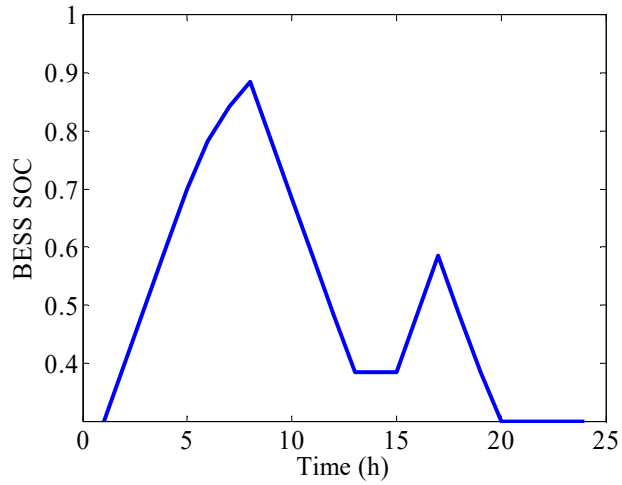

Fig. 12: LAB state of charge (1/5/2017).

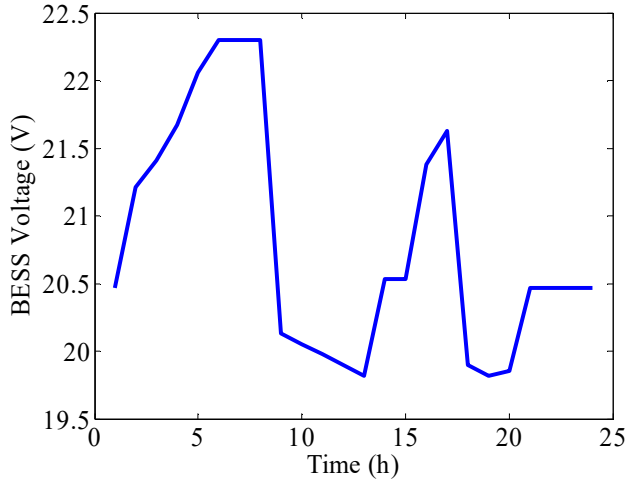

Fig. 13: LAB voltage (1/5/2017).

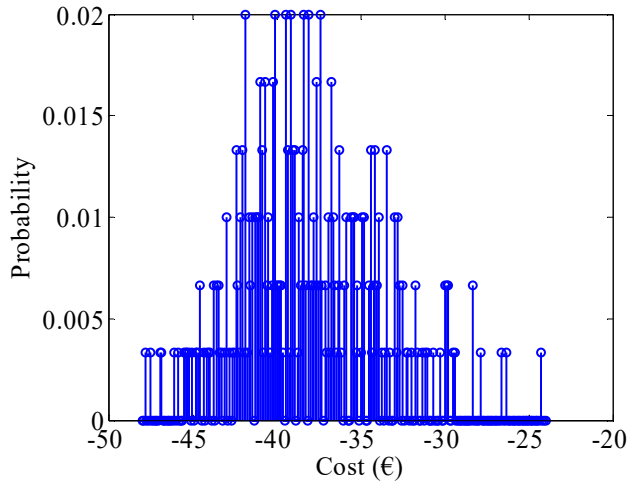

Fig. 14: LAB operating cost (1/5/2017).

5.4 Control of VRFB for January 5th, 2017

In this subsection, VRFB bank operation is analysed in order to determine the scheduling and dynamic behaviour in terms of battery bank power, SOC, and voltage. The matrix for probabilistic optimization in shown in Table 9, where the charging period between t= 3 and t= 7, which does not depend on the price uncertainty, can be easily recognized. On the other hand, the discharging hours can be recognized by their high probability; specifically, between t= 19 and t= 23.

Table 9: Matrix of probabilistic optimization (VRFB).

t	$f_{BS,t}(BS_t = 1)$	$f_{BS,t}(BS_t = -1)$	$f_{BS,t}(BS_t = 0)$	BS_t
1	0	0.5466	0.4533	-1
2	0.4866	0.2766	0.2366	1
3	1	0	0	1
4	1	0	0	1
5	1	0	0	1
6	1	0	0	1
7	1	0	0	1
8	0.0800	0.1100	0.8100	0
9	0	0.6566	0.3433	-1
10	0	0.8600	0.1400	-1
11	0	0.8733	0.1266	-1
12	0	0.8100	0.1900	-1
13	0.0033	0.6400	0.3566	-1
14	0	0.6166	0.3833	-1
15	0.0566	0.4366	0.5066	0
16	0.4600	0.0866	0.4533	1
17	0.2900	0.0800	0.6300	0
18	0.0033	0.5566	0.4400	-1
19	0	0.9866	0.0133	-1
20	0	0.9933	0.0066	-1
21	0	0.9800	0.0200	-1
22	0	0.9733	0.0266	-1
23	0	0.9233	0.0766	-1
24	0	0.8733	0.1266	-1

Based on the results presented in Table 9 related to the battery bank scheduling, the completed simulation of VRFB-bank operation was carried out using the formulation discussed in subsection 3.2 and resulted in the profiles shown in Figs. 15-17 for battery power, SOC, and voltage, respectively.

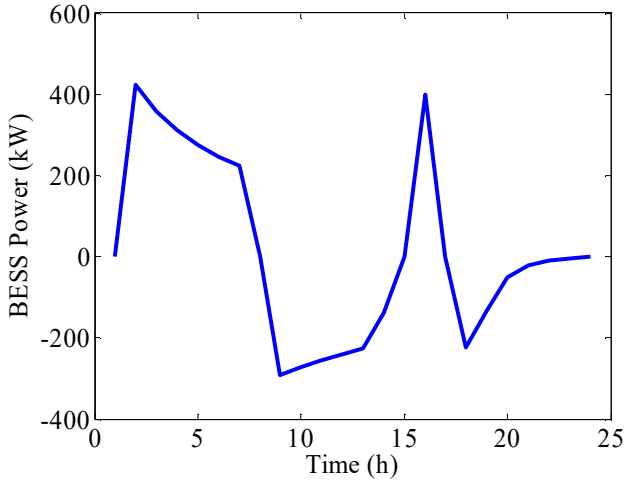

Fig. 15: VRFB power (1/5/2017).

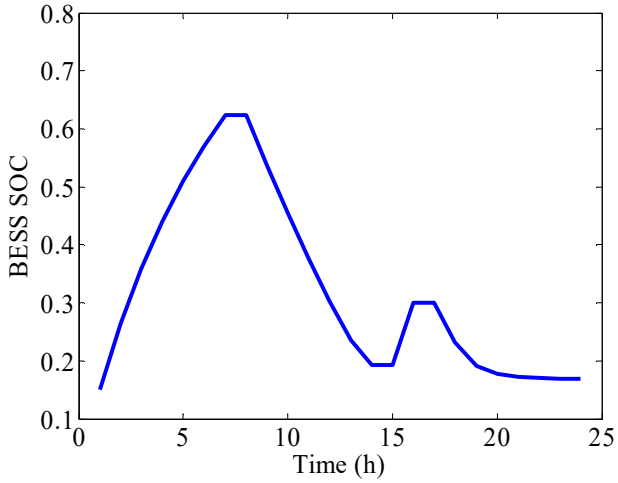

Fig. 16: VRFB state of charge (1/5/2017).

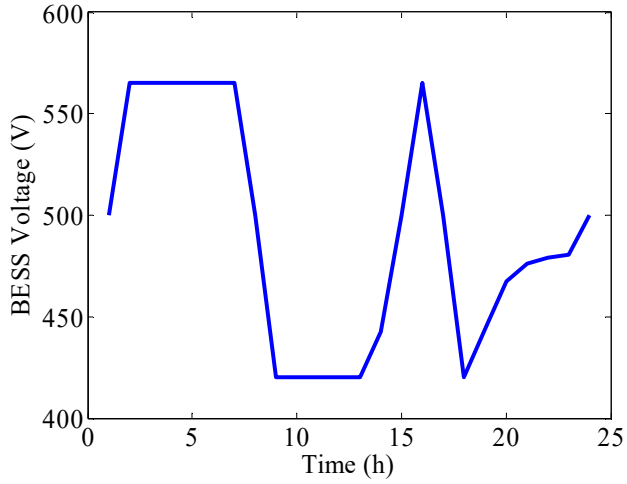

Fig. 17: VRFB voltage (1/5/2017).

Fig. 18 shows the probability mass function of operating cost for this storage technology, which is also influenced by the beta distribution used to represent the forecasting error.

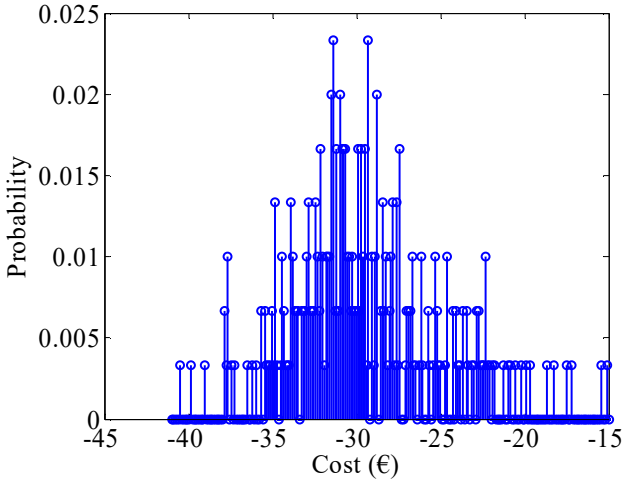

Fig. 18: VRFB operating cost (1/5/2017).

Table 10 presents the extreme and average values of the revenue for each technology, as well as its actual value. These extreme values were directly obtained from the CDF of distributions presented in Figs. 14 and 18 considering a significance level of 5%. It is possible observing how the proposed model is able to estimate an interval with a reasonable level of reliability; the interval could be extended by considering a significance level closer to zero.

In addition, from the analysis of Figs. 11 and 15 combined with Table 10, it is possible to observe that the LAB bank exchanges less power with the SG than the VRFB bank does; however, the LAB bank results in higher revenue than that estimated from the operation of VRFB bank. These results reveal the importance of considering the variable efficiency of each battery technology as well as the power converter. The efficiency of LAB bank is mainly influenced by gassing current during the charging process, while the efficiency of the VRFB bank is influenced by circulation pumps, among other instruments and devices. On average, the computation required to solve this problem took 44.732 minutes.

Table 10: Extreme and average values of operating cost (1/5/2017).

Cost	LAB	VRFB
Minimum (€)	-45.493976	-37.763052
Average (€)	-38.554217	-30.349398
Maximum (€)	-29.590361	-20.012048
Actual (€)	-44.300481	-19.483770

Finally, as the interest in researching the interaction between distributed storage systems and SG has been growing [39-41]. The proposed approach could be extended to control a storage system aggregator taking into account the limitations related to distribution network in terms of voltage profile and power flow.

6. Conclusions

In this paper, a novel probabilistic optimization model for the control of LABs and VRFBs enrolled in real-time pricing programs that takes into account the forecasting error of electricity prices has been presented. It has been numerically illustrated by analysing a representative case study of a 2 MWh storage system operating in the Spanish electricity market. Relevant factors and phenomena related to LAB operation, such as the gassing process, as well as VRFB charging and discharging efficiencies have been carefully included on the energy arbitrage problem, which allowed reliable prediction intervals in the estimation of daily revenue according to a determined significance level. In addition, the comparison of LABs and VRFBs under similar operating conditions has shown the importance of operating conversion efficiency, which varies with the charging and discharging of power and is frequently represented by a constant value in many works found in the technical literature.

Acknowledgement

This work was supported by FEDER funds through COMPETE 2020 and by Portuguese funds through FCT, under Projects SAICT-PAC/0004/2015 - POCI-01-0145-FEDER-016434, POCI-01-0145-FEDER-006961, UID/EEA/50014/2013, UID/CEC/50021/2013, UID/EMS/00151/2013 and SFRH/BPD/103079/2014. Also, the research leading to these results has received funding from the EU Seventh Framework Programme FP7/2007-2013 under grant agreement no. 309048. Moreover, this work was supported by the Ministerio de Economía y Competitividad of the Spanish Government under research Project ENE2013-48517-C2-1-R.

References

[1] Lucas A, Chondrogiannis S. Smart grid energy storage controller for frequency regulation and peak shaving, using a vanadium redox flow battery. International Journal of Electrical Power & Energy Systems 2016;80:26-36.

[2] Zafirakis D, Chalvatzis KJ, Baiocchi G, Daskalakis G. The value of arbitrage for energy storage: Evidence from European electricity markets. Appl Energ 2016;184:971-986.

[3] Bussar C, Stöcker P, Cai Z, Moraes LJ, Magnor D, Wiernes P, van Bracht N, Moser A, Sauer DU. Large-scale integration of renewable energies and impact on storage demand in a European renewable power system of 2050 – Sensitivity study. J Energy Storage 2016;6:1-10.

[4] Bradbury K, Pratson L, Patiño-Echeverri D. Economic viability of energy storage systems based on price arbitrage potential in real-time US electricity markets. Appl Energ 2014;114:512-519.

[5] de Sisternes FJ, Jenkins JD, Botterud A. The value of energy storage in decarbonizing the electricity sector. Appl Energ 2016;175:368-379.

[6] Dunbar A, Cradden LC, Wallace R, Harrison GP. Impact of wind power on arbitrage revenue for electricity storage. IET Gener Transm Dis 2016;10(3):798-806.

[7] Weitemeyer S, Kleinhans D, Vogt T, Agert C. Integration of renewable energy sources in future power systems: The role of storage. Renew Energ 2015;75:14-20.

[8] McConnell D, Forcey T, Sandiford M. Estimating the value of electricity storage in an energy-only wholesale market. Appl Energ 2015;159:422-432.

[9] Powell KM, Kim JS, Cole WJ, Kapoor K, Mojica JL, Hedengren JD, Edgar TF. Thermal energy storage to minimize cost and improve efficiency of a polygeneration district energy system in a real-time electricity market. Energy 2016;113:52-63.

[10] Tan X, Wu Y, Tsang DHK. Pareto optimal operation of distributed battery energy storage systems for energy arbitrage under dynamic pricing. IEEE Trans Parallel Distrib Syst 2016;27(7):2103-2115.

[11] Zhang Z, Wang J, Ding T, Wang X. A two-layer model for microgrid real-time dispatch based on energy storage system charging/discharging hidden costs. IEEE Trans Sustain Energy 2017;8(1):33-42.

[12] Kim H, Heo J-H, Park J-Y, Yoon YT. Impact of battery energy storage system operation strategy on power system: An urban railway load case under a time-of-use tariff. Energies 2017;10(1):1-15.

[13] Dvorkin Y, Fernández-Blanco R, Kirschen DS, Pandžić H, Watson J-P, Silva-Monroy CA. Ensuring profitability of energy storage. IEEE Trans Power Syst 2017;32(1):611-623.
[14] Xu Y, Tong L. Optimal operation and economic value of energy storage at consumer locations. IEEE Trans Autom Control 2017;62(2):792-807.
[15] Sakti A, Gallagher KG, Sepulveda N, Uckun C, Vergara C, de Sisternes FJ, Dees DW, Botterud A. Enhanced representations of lithium-ion batteries in power systems models and their effect on the evaluation of energy arbitrage applications. J Power Sources 2017;342:279-291.
[16] Geem ZW, Yoon Y. Harmony search optimization of renewable energy charging with energy storage system. Int J Elec Power 2017;86:120-126.
[17] Wankmüller F, Thimmapuram PR, Gallagher KG, Botterud A. Impact of battery degradation on energy arbitrage revenue of grid-level energy storage. J Energy Storage 2017;10:56-66.
[18] Lujano-Rojas JM, Dufo-López R, Bernal-Agustín JL, Catalão JPS. Optimizing daily operation of battery energy storage systems under real-time pricing schemes. IEEE Trans Smart Grid 2017;8(1):316-330.
[19] Contreras J. Forecasting models of electricity prices. Energies 2017;10:1-2.
[20] Weron R. Electricity price forecasting: A review of the state-of-the-art with a look into the future. Int J Forecasting 2014;30:1030-1081.
[21] Rosenblatt M. Remarks on a multivariate transformation. Ann Math Stat 1952;23(3):470-472.
[22] Barbiero A. A general discretization procedure for reliability computation in complex stress-strength models. Math Comput Simulat 2012;82(9):1667-1676.
[23] Brown BG, Katz RW, Murphy AH. Time series models to simulate and forecast wind speed and wind power. J Clim and Appl Meteorol 1984;23(8):1184-1195.
[24] Schwarz G. Estimating the dimension of a model. Ann Stat 1978;6(2):461-464.
[25] Akaike H. A new look at the statistical model identification. IEEE Trans Autom Control 1974;19(6):716-723.
[26] Ljung GM, Box GEP. On a measure of lack of fit in time series models. Biometrika 1978;65(2):297-33.
[27] Goldberg DE. Genetic algorithms in search, optimization and machine learning. 1st ed. Boston, MA, USA: Addison-Wesley Longman Publishing Co, Inc; 1989.
[28] Maciejowska K, Nowotarski J, Weron R. Probabilistic forecasting of electricity spot prices using factor quantile regression averaging. Int J Forecasting 2016;32:957-965.
[29] Bello A, Renesses J, Muñoz A, Delgadillo A. Probabilistic forecasting of hourly electricity prices in the medium-term using spatial interpolation techniques. Int J Forecasting 2016;32:966-980.
[30] Lamber T, Gilman P, Lilienthal P. Micropower system modeling with HOMER. In: Integration of alternative sources of energy. John Wiley & Sons; 2006. Pp. 379-418.
[31] Schreiber M, Harrer M, Whitehead A, Bucsich H, Dragschitz M, Seifert E, Tymciw P. Practical and commercial issues in the design and manufacture of vanadium flow batteries. J Power Sources 2012;206:483-489.
[32] Schiffer J, Sauer DU, Bindner H, Cronin T, Lundsager P, Kaiser R. Model prediction for ranking lead-acid batteries according to expected lifetime in renewable energy systems and autonomous power-supply systems. J Power Sources 2007;168:66-78.
[33] Qiu X, Nguyen TA, Guggenberger JD, Crow ML, Elmore AC. A field validated model of a vanadium redox flow battery for microgrids. IEEE Trans Smart Grid 2014;5(4):1592-1601.
[34] Nguyen TA, Qiu X, Guggenberger JD, Crow ML, Elmore AC. Performance characterization for photovoltaic-vanadium redox battery microgrid systems. IEEE Trans Sustain Energy 2014;5(4):1379-1388.
[35] Nguyen TA, Crow ML, Elmore AC. Optimal sizing of a vanadium redox battery system for microgrid systems. IEEE Trans Sustain Energy 2015;6(3):729-737.
[36] Turker B, Klein SA, Hammer E-M, Lenz B, Komsiyska. Modeling a vanadium redox flow battery system for large scale applications. Energ Convers Manage 2013;66:26-32.
[37] Rampinelli GA, Krenzinger A, Romero FC. Mathematical models for efficiency of inverters used in grid connected photovoltaic systems. Renew Sust Energ Rev 2014;34:578-587.
[38] Spanish electricity market, https://www.esios.ree.es/es; 2015 [accessed 02.23.2017].
[39] Lakshminarayana S, Quek TQS, Poor HV. Cooperation and storage tradeoffs in power grids with renewable energy resources. IEEE J Sel Areas Commun 2014;32(7):1386-1397.
[40] Lakshminarayana S, Xu Y, Poor HV, Quek TQS. Cooperation of storage operation in a power network with renewable generation. IEEE Trans Smart Grid 2016;7(4):2108-2122.
[41] Kwon S, Xu Y, Gautam N. Meeting inelastic demand in systems with storage and renewable sources. IEEE Trans Smart Grid 2017;8(4):1619-1629.